https://doi.org/10.1016/j.jclepro.2022.135200

3D radially-grown TiO_2 nanotubes/Ti mesh photoanode for photocatalytic fuel cells towards simultaneous wastewater treatment and electricity generation

Yuxin Liu [a,b], Rong Chen [a,b]*, Xun Zhu [a,b], Dingding Ye [a,b], Yang Yang [a,b], Jinwang Li [a,b], Dechao Wang [a,b], Liang An [c], Qiang Liao [a,b]

[a] Key Laboratory of Low-grade Energy Utilization Technologies and Systems (Chongqing University), Ministry of Education, Chongqing 400030, China

[b] Institute of Engineering Thermophysics, School of Energy and Power Engineering, Chongqing University, Chongqing 400030, China

[c] Department of Mechanical Engineering, The Hong Kong Polytechnic University, Hung Hom, Kowloon, Hong Kong, China

* Corresponding author

[a,b] Tel.: 0086-23-65102019; fax: 0086-23-65102474; e-mail: rchen@cqu.edu.cn (Rong Chen)

Abstract

Photocatalytic fuel cell (PFC) represents a clean environment and energy technology to directly recover chemical energy contained in wastewater for electricity generation by using solar energy. It is advantageous for the PFC to adopt the TiO_2 nanotube array photoanodes that usually grow on planar Ti substrates. But low specific surface area and light utilization limit the improvement in the PFC performance. This work is directed to the development of a 3D radially-grown TiO_2 nanotubes/Ti mesh photoanode. The Ti mesh substrate provides a large specific surface area for growing TiO_2 nanotubes and benefits light scattering, while TiO_2 nanotubes with high length-

diameter ratio enhances electron transfer. Because of these merits, the staggered PFC with the 3D radially-grown TiO_2 nanotubes/Ti mesh photoanode yields a maximum power density (P_{MAX}) of ~ 0.074 mW/cm^2, which is about 6.2 and 1.6 times as those with the TiO_2 nanoparticles/Ti mesh and TiO_2 nanotubes/Ti foil photoanodes, respectively. Increasing the mesh density of Ti mesh is synergic to improve the cell performance due to increased surface area and light utilization. The optimal P_{MAX} of the ordinary PFC reaches as high as 0.15 mW/cm^2 when using the Ti mesh of 300 per inch. Notably, using Ti mesh as a substrate makes it easy to integrate multiple Ti meshes to form a stacked 3D photoanode, which shows excellent performance when feeding various pollutants even with biogas slurry. Besides, good stability of the developed photoanode is also demonstrated. This work offers an innovative strategy for developing high-performance 3D structured photoanode for photoelectrochemical systems.

Keywords: 3D radially-grown TiO_2 nanotubes/Ti mesh photoanode; Mesh density; Stacked photoanode; Photocatalytic fuel cell

1 Introduction

A huge amount of organic pollutants has been discharged into natural water body in accompany with rapid industrialization, resulting in serious water pollution (Barbosa et al., 2016). In order to effectively solve water pollution problem, various sewage treatment technologies including physical, chemical, and biological methods, have been developed (Saravanan et al., 2021). In the past, wastewater as an environment problem needs energy to remove contaminants, ignoring abundant chemical energy contained in wastewater (Li et al., 2015). Photocatalytic fuel cell (PFC) represents one of the advanced technologies for simultaneous wastewater treatment and electricity generation by using solar energy (He et al., 2018). This technology can realize the recovery of waste resources into clean energy, contributing to sustainability of environment and energy. In fundamental, generation and transfer of photo-excited carriers in the photoanode decisively determines the PFC performance (Zeng et al., 2018). Thus, the development of a high-performance photoanode plays a dominant role in boosting the PFC performance. Among existing semiconductor photocatalysts used in PFCs, TiO_2 has been the most-commonly used because it is non-toxic, chemically stable and cost-effective (Chen et al., 2020a). Especially, highly-ordered TiO_2 nanotube arrays prepared by electrochemical anodization has been demonstrated to have extraordinarily excellent electron mobility in a confined path (Liu et al., 2009a). Ye et al. (2018) constructed a membrane-free PFC with the TiO_2 nanotubes prepared on a Ti foil as the photoanode, which showed significantly enhanced MCPA removal. Lin et al.

(2020) developed a TiO_2 nanotube arrays photoanode prepared by the anodizing treatment of Ti foil to enhance the performance of a microfluidic all-vanadium photoelectrochemical cell. It is obvious that in-situ grown TiO_2 nanotube array by electrochemical anodization is a promising approach for the development of high-performance photoanode.

In previous works (Wang et al, 2020b; Zhao et al., 2017), TiO_2 nanotubes are usually grown in planar Ti substrates, such as Ti plate and Ti foil. Due to low specific surface area of these planar substrates, the growth of TiO_2 nanotubes is limited, resulting in low solar energy utilization (Liu et al., 2011). Different from planar substrates, Ti mesh composed of many overlapped Ti wires has a larger specific surface area (Bao et al., 2018). The growth of the TiO_2 nanotubes on the Ti mesh exhibited radial orientation, forming a three-dimensional (3D) structure, which not only provided more active sites but also benefited light scattering (Liao et al., 2012). Liu et al. (2009b) prepared the vertically-oriented TiO_2 nanotube arrays on Ti mesh as flexible electrodes for dye-sensitized solar cells, which yielded a conversion efficiency of 1.23%. Martin et al. (2017) reported the highly photoactive TiO_2 nanotubes on Ti mesh for photocatalytic NO_X removal; excellent photo-activities in both gaseous and liquid phases were achieved. Besides, Qiu et al. (2018) prepared TiO_2 nanotubes on Ti mesh and demonstrated its ability for various pollutants. Lashkov et al. (2020) reported a Ti wire functionalized with inherent anatase TiO_2 nanotubes to serve as a one-electrode gas

sensor. Except one layer of Ti mesh, Sopha et al. (2021) prepared TiO_2 nanotubes on Ti meshes fabricated by direct ink writing and the surface area for the growth of TiO_2 nanotube layers could be further increased. However, few attempts have been made to apply the Ti mesh with TiO_2 nanotubes to the photoanode of a PFC. Little is known on the effect of the grid structure of Ti mesh on the photoanode performance, and its applicability in PFCs for actual wastewater treatment and electricity generation.

In this study, a photoanode with radially-oriented TiO_2 nanotubes on Ti mesh was developed for a PFC by electrochemical anodization. A stacked photoanode with multiple TiO_2 nanotubes grown Ti meshes was also proposed. Therefore, the developed photoanode could be termed as 3D radial TiO_2 nanotubes/Ti mesh photoanode. The performance evaluation was conducted in a single-chamber photocatalytic fuel cell. In addition, the effect of Ti mesh density was investigated. Finally, the feasibility of a PFC with the newly-developed photoanode was demonstrated by using various pollutants and actual biogas slurry for simultaneous electricity generation and pollutant degradation. The results obtained in this work are informative for the design and operation of this type of photoanode used in various photoelectrochemical systems.

2 Experimental Section

2.1 Preparation of photoanode

The 3D radial TiO_2 nanotubes/Ti mesh photoanode was fabricated by the

electrochemical anodization with a constant anodizing voltage. Before anodization, Ti meshes (mesh density: 80, 150 and 300 per inch) with a size of 1.5 cm × 1.5 cm were cleaned ultrasonically with ethanol, acetone, and deionized water to remove the surface impurities. Subsequently, Ti meshes were immersed in a mixture solution of HF and HNO_3 acid (HF: HNO_3: H_2O= 1:4:10 in volume) for 10 s, and then cleaned ultrasonically with deionized water. The anodization was carried out in a two-electrode electrochemical configuration with the pretreated Ti meshes as the working electrode and a graphite plate as the counter electrode at 40 V for 3 h. The electrolyte was an ethylene glycol solution containing 0.3 wt % NH_4F and 5 vol % H_2O. Afterwards, the samples were immersed in ethylene glycol solution for 12 h to remove the fluoride compounds (Hu et al., 2008; Yang et al., 2011), and then in deionized water for 60 s. Finally, the samples were annealed in a tube furnace at 450 °C for 3 h under air atmosphere with a ramping rate of 5 °C/min. For comparison, a photoanode with TiO_2 nanotubes grown on the Ti foil was prepared under the same conditions to demonstrate the advantage of the Ti mesh structure, termed as TiO_2 nanotubes/Ti foil photoanode. Commercial P25 nanoparticles have been widely used to prepare the PFC photoanode. Hence, a photoanode with TiO_2 nanoparticles directly coated onto the Ti mesh was also prepared by wet spraying method to demonstrate the advantage of the TiO_2 nanotubes, termed as TiO_2 nanoparticles/Ti mesh photoanode.

2.2 Characterizations

The microstructures of the prepared photoanodes were obtained by scanning electron microscopy (SEM, Hitachi SU8020) and transmission electron microscopy (TEM, FEI Tecnai G2 F30). The crystal phases of the photoanodes were investigated by X-ray diffractometry (XRD, BRUKE D8 ADVANCE). The UV-vis diffuse reflectance spectra (UV-vis DRS, Hitachi UV3600) were obtained using $BaSO_4$ as the reference background. The Brunaure-Emmett-Teller (BET) surface areas of the photoanodes were obtained by a N_2 adsorption/desorption analyzer (ASAP 2460). Free radicals ($\cdot OH$ and $\cdot O_2^-$) were characterized by the electron paramagnetic resonance (EPR, BRUKER A300-10/12) using DMPO under illumination. The photocurrent response, electrochemical impedance spectroscopy (EIS) and CV test of these photoanodes were characterized in a standard three-electrode system by an electrochemical workstation (ZAHNER-elektrik GmbH & CoKG). Here, the prepared photoanodes were functioned as the working electrode, Pt electrode as the counter electrode and Ag/AgCl electrode as the reference electrode. The electrolyte contained 1.0 M KOH (90%, Aladdin) and 10 mg/L Methyl orange (MO). A UV-LED light (HTLD-S60-365, China) was used as a light source and the light intensity was 5 mW/cm^2 measured by a UV radiometer (UV-A, Photoelectric Instrument Factory of Beijing Normal University). Electrochemical impedance spectroscopy (EIS) measurements were performed over a frequency range of 0.01~100000 Hz. Besides, the electrolyte containing 0.5 M Na_2SO_4 and 10 mg/L MO was also used to investigate the influence of pH value.

2.3 Photocatalytic degradation

MO was used as a model pollutant to evaluate the photocatalytic activity of the prepared photoanodes. Before irradiation, the photoanodes were immersed in the 2.5 mL solution (1.0 M KOH and 10 mg/L MO) under dark condition with moderate stirring for 30 min to achieve adsorption-desorption equilibrium. These photoanodes were then irradiated by UV light (5 mW/cm^2) for 1 h. Typically, the MO degradation efficiency was determined by

$$\text{degradation efficiency} = \frac{C_0 - C_t}{C_0} \times 100\% \quad (1)$$

where C_o was the initial absorbance of MO, and C_t was the absorbance of MO after a running time t, both of which were measured by an Ultraviolet-Visible spectrophotometer (TU-1950, Persee, China) at a wavelength of 465 nm.

2.4 Construction and evaluation of PFC

The constructed single-chamber PFCs with the as-prepared photoanodes and Pt/C air-breathing cathode are illustrated in **Fig. 1**. In this work, we designed two PFCs for evaluating the cell performance. In the first design (**Fig. 1a**), the photoanode and air-breathing cathode were staggered, termed as staggered PFC, where the light was irradiated to the photoanode through the solution. This is because light cannot pass through the TiO_2 nanotubes/Ti foil photoanode. Such design and illumination mode allowed for fair comparison between the photoanodes prepared on various substrates.

The second design was an ordinarily-designed PFC (**Fig. 1b**), termed as ordinary PFC, in which the photoanode and air-breathing cathode were arranged face-to-face and the light was irradiated to the photoanodes from the back cover. This design was mainly used for evaluating the performance of the PFC with the Ti mesh based photoanodes. In the operation, the PFCs were filled with 2.5 mL fuel-electrolyte mixture. Different organic pollutants (10 mg/L MO, 0.2 M methanol or 100% biogas slurry) were used as the fuel resources and 1 M KOH was used as the supporting electrolyte. The PFC performances were measured with an electronic load (Xinwei CT-3008). The change of chemical oxygen demand (COD) of biogas slurry was measured by a spectrophotometer (Hach DR3900, USA).

3 Results and Discussion

The photoanode with 3D radial TiO_2 nanotubes grown on the Ti mesh with a mesh density of 150 per inch was chosen a typical sample for material characterizations. **Fig. 2a** shows the well-aligned nanotube arrays on the Ti mesh. They were quite uniform with an outer diameter of about 109 nm and an inner diameter of about 84 nm and a length of about 6.7 μm. Different from the perpendicularly grown TiO_2 nanotubes on the planar Ti foil (**Fig. S1**) and the aggregated TiO_2 nanoparticles on the Ti mesh (**Fig. S2**), the TiO_2 nanotubes radially grew on the Ti mesh shown in **Fig. 2b**. The dimensions of the TiO_2 nanotubes on different substrates are detailed in **Table S1**. The outer and inner diameters of the TiO_2 nanotubes grown on the Ti mesh and foil were quite similar

due to the same anodizing voltage. In addition, the TiO_2 nanotube bundles and some cracks between the bundles were observed (**Fig. S3**). This was attributed to the lateral deflection of the TiO_2 nanotubes caused by van der Waals attraction and capillary force during drying (Zhu et al., 2007). The top of the TiO_2 nanotube bundles was prone to collapse. Therefore, the length of the TiO_2 nanotubes grown on the Ti mesh was slightly shorter than that of the Ti foil, which was consistent with the results by Ocampo and Echeverria (2021). The shorter length of the TiO_2 nanotubes on the Ti mesh and the lower apparent area of the substrate resulted in lower mass of the TiO_2 nanotubes than that on the Ti foil (**Table S1**). However, the radial growth resulting from the Ti wire structure gave rise to a higher specific surface area (**Fig. 2c**). As a result, the use of the Ti mesh for the growth of the TiO_2 nanotubes can address the issue of the limited specific surface area by the planar substrate. Besides, the in-situ grown TiO_2 nanotubes had a higher exposed area than the aggregated TiO_2 nanoparticles on the Ti mesh. **Figs. 2d** and **2e** show the TEM image and XRD pattern of the 3D radial TiO_2 nanotubes/Ti mesh photoanode. As shown in **Fig. 2d**, the TiO_2 nanotubes were evenly packed together, which was consistent with the SEM result. The HRTEM image (inserted in **Fig. 2d**) showed that the crystalline spacing of the nanotubes was about 0.35 nm, corresponding to the (101) plane of the anatase phase (Sankapal et al., 2005). According to the XRD pattern, the characteristic diffraction peaks labeled “T” at 35.1°, 38.5°, 40.3°, 53.1°, 62.9°, 70.7°, 76.1°, 77.2° can be assigned to the Ti substrate; and the peaks labeled “A” at the diffraction peaks of 25.4°, 38.0°, 48.2° and 53.9° correspond to the

(101), (004), (200), and (105) crystal faces of anatase-phase TiO_2 (Liu et al., 2008). The above XRD and TEM results indicate that the crystal structure of the TiO_2 nanotubes on the Ti mesh is anatase phase, which has good photocatalytic capacity (Sivalingam et al., 2003). The TiO_2 nanoparticles were mainly composed of a large amount of anatase TiO_2 and a small amount of rutile TiO_2 (**Fig. S4**). In addition, the light absorption of the 3D radial TiO_2 nanotubes/Ti mesh photoanode was investigated by ultraviolet–visible diffuse reflection spectra (UV–vis DRS) shown in **Fig. 2f**. The TiO_2 nanotubes mainly absorbed ultraviolet light with the wavelength below 400 nm and the band gap was approximately 3.02 eV determined by Tauc plot method (Tauc et al., 1966).

Methyl orange (MO) is one of the most widely used dyes, which has a stable azoic structure and weak adsorption on the photocatalysts due to the surface charge property of TiO_2 under alkaline and neutral conditions (O'Shea et al., 1999), leading to difficulty in complete decomposition. Therefore, MO was used as a model pollutant to investigate the photocatalytic and photoelectrochemical performances of the prepared photoanodes. First of all, we compared the photocatalytic and photoelectrochemical performances of the developed 3D radial TiO_2 nanotubes/Ti mesh photoanode under the alkaline and neutral conditions. Here, the 3D radial TiO_2 nanotubes/Ti mesh with a mesh density of 300 per inch was used due to large specific surface area and high light utilization, which will be discussed later. As shown in **Fig. S5a** and **S5b**, MO was more efficiently degraded and a higher photoelectrochemical performance was yielded under the

alkaline condition than did neutral condition due to more efficient capture of photo-excited holes, which could also be confirmed by small impedance shown in **Fig. S5c.** According to the EPR results (**Fig. S6**), more $\cdot OH$ and $\cdot O_2^-$ were generated under alkaline condition than did neutral condition. It is indicated that more holes were captured for photocatalytic/photoelectrochemical reactions, thereby boosting the performance under alkaline condition. This result is consistent with the data reported by Liao et al. (2012). Therefore, the operation under the alkaline condition was chosen in the follow-up work. The degradation performances of the prepared photoanodes (3D radial TiO_2 nanotubes/Ti mesh photoanode, TiO_2 nanotubes/Ti foil photoanode, TiO_2 nanoparticles/Ti mesh photoanode) were compared under the same conditions of 2.5 mL, 10 mg/L MO, 1.0 M KOH and 5 mW/cm^2 UV light intensity. As shown in **Fig. 3a**, all these photoanodes were active in degrading MO. These photoanodes exhibited dramatic decrease of the MO concentration after 1 h. The degradation efficiency by the 3D radial TiO_2 nanotubes/Ti mesh photoanode reached about 92%, presenting the improvements by 37% and 14% over the TiO_2 nanotubes/Ti foil and TiO_2 nanoparticles/Ti mesh, respectively. In addition, the photolytic removal by UV light irradiation and the adsorption under dark condition were negligible (**Fig. 3a**), confirming that the MO removal was mainly caused by photocatalytic degradation. The photocatalytic reaction rate constants, *k*, can also be obtained by the fitting with the pseudo-first-order kinetic model and the results are shown in **Fig. 3b**. The apparent photocatalytic reaction rate constant of the 3D radial TiO_2 nanotubes/Ti mesh

photoanode was about 0.041±0.001 min^{-1}, which was about 2.3 and 1.4 times higher than the TiO_2 nanotubes/Ti foil (0.018±0.001 min^{-1}) and TiO_2 nanoparticles/Ti mesh (0.029±0.003 min^{-1}) photoanodes, indicating excellent photocatalytic performance of the 3D radial TiO_2 nanotubes/Ti mesh photoanode.

The photocurrent responses and electrochemical impedances of these photoanodes were investigated in a three-electrode system to evaluate their photoelectrochemical activities. It can be seen from **Fig. 3c** that all samples exhibited a negligible current in dark, while the photocurrent densities raised rapidly upon UV light irradiation. The 3D radial TiO_2 nanotubes/Ti mesh photoanode possessed the highest photocurrent density (0.23 mA/cm^2) in the tested five cycles, which was approximately 1.2 times as the TiO_2 nanotubes/Ti foil (0.19 mA/cm^2) and 8.2 times as the TiO_2 nanoparticles/Ti mesh (0.028 mA/cm^2), respectively. The Nyquist curves and equivalent circuit are shown in **Fig. 3d**. The 3D radial TiO_2 nanotubes/Ti mesh photoanode showed the smallest impedance. With the equivalent circuit model, the charge transfer resistances of the 3D radial TiO_2 nanotubes/Ti mesh, TiO_2 nanoparticles/Ti mesh and TiO_2 nanotubes/Ti foil photoanodes could be estimated, which were 424.5 Ω, 1412.0 Ω and 548.4 Ω, respectively. The 3D radial TiO_2 nanotubes/Ti mesh photoanode exhibited the smallest charge transfer resistance, suggesting more efficient separation of electrons and holes and faster charge transfer. Generally, the improvements in the photocatalytic and photoelectrochemical performances by the newly-developed photoanode can be

attributed to the grid structure of Ti mesh and radially-grown TiO_2 nanotube arrays. Compared to the planar substrate of the Ti foil, the grid structure of Ti mesh could not only provide higher electrochemical surface area (**Fig. S7**) and more path for reactant transport, but also effectively absorb the incident photons from all directions (Luo et al., 2019). In addition, TiO_2 nanoparticles are densely packed on the Ti mesh by wet spraying (**Fig. S2**), which was not conducive to the separation of photogenerated electrons and holes as compared with TiO_2 nanotubes (Lin et al., 2020). As a consequence, choosing Ti mesh as a substrate to in-situ grow radial TiO_2 nanotubes is a promising strategy for developing high-performance photoanode.

The developed photoanodes were also evaluated by incorporating them into a single-chamber photocatalytic fuel cell (staggered PFC) for simultaneous pollutant degradation and electricity generation. The running conditions were the same as above. The current-voltage (*J-V*) and the current-power (*J-P*) plots of the PFCs using different photoanodes are shown in **Fig. 4a** and **4b**. It can be found that the short-circuit current density J_{SC} of the staggered PFC using the 3D radial TiO_2 nanotubes/Ti mesh photoanode (meth density: 300 per inch) was higher than the TiO_2 nanotubes/Ti foil and TiO_2 nanoparticles/Ti mesh. The staggered PFC with the 3D radial TiO_2 nanotubes/Ti mesh photoanode yielded the highest power density P_{MAX} (0.074 mW/cm^2). Obviously, the overall discharging performance of the PFC with the 3D radial TiO_2 nanotubes/Ti mesh photoanode was more excellent than did the others. As

mentioned above, this can be ascribed to the enhanced light energy utilization and increased specific surface area as a result of radial growth of TiO_2 nanotubes and grid structure of Ti mesh. In addition, the MO removal efficiencies in the PFC operation mode were also compared. Here, the degradation of MO was performed at a constant cell voltage of 0.3 V. As shown in **Fig. 4c**, the degradation efficiencies of MO were only around 56% and 73% for the staggered PFC with the TiO_2 nanotubes/Ti foil and TiO_2 nanoparticles/Ti mesh photoanodes, respectively, while it was as high as 88% for the 3D radial TiO_2 nanotubes/Ti mesh photoanode. The above results indicate that the 3D radial TiO_2 nanotubes/Ti mesh photoanode is capable of yielding superior performance for simultaneous organics degradation and electricity generation.

It is worth noting that the performances of the same photoanode in the staggered and ordinary PFCs were different. The J_{SC} and P_{MAX} of the ordinary PFC using the 3D radial TiO_2 nanotubes/Ti mesh photoanode (mesh density: 300 per inch) were 0.49 mA/cm^2 and 0.15 mW/cm^2, which was higher than the one used in the staggered PFC. The degradation efficiency of MO for the ordinary PFC with the 3D radial TiO_2 nanotubes/Ti mesh photoanode was much higher than that staggered PFC. This is mainly due to light attenuation caused by the MO solution. As mentioned above, the light should irradiate to the TiO_2 nanotubes/Ti foil photoanode because the Ti foil is opaque (Lin et al., 2020). The implementation of the staggered PFC was then adopted for fair comparison, in which the photoanodes were irradiated from the side of the MO

solution instead of the transparent back cover in the ordinary PFC, leading to inevitable light attenuation. Meanwhile, the reactants and light could more easily reach the entire surface of the photoanodes used in the ordinary PFC. Therefore, the ordinary PFC showed better performance, which was then used to study the photoanodes with the Ti mesh as a substrate in the following.

The above results have confirmed that the in-situ grown TiO_2 nanotubes using Ti mesh as a substrate is an advantageous method to improve the photoanode performance. No doubt, the structure of Ti mesh, i.e., mesh density, greatly affects the surface area for the growth of TiO_2 nanotubes and mass transfer and light absorption. Therefore, the effect of the mesh density of Ti mesh was investigated. Three 3D radial TiO_2 nanotubes/Ti mesh photoanodes with different mesh densities (80, 150 and 300 per inch) were prepared. As shown in **Fig. 5a**, the photocatalytic degradation efficiency increased with increasing the mesh density from 80 to 300 per inch, similar to the previously reported data (Delavari and Amin, 2016). The maximum degradation efficiency of MO under UV-light irradiation for 1 h could reach about 92% for the Ti mesh with a mesh density of 300 per inch, and the corresponding photocatalytic reaction rate constant was around 0.041 ± 0.001 min^{-1}. The reasons leading to the improvement in the photoanode performance with increasing the mesh density can mainly fall into two aspects. The Ti mesh with a mesh density of 300 per inch has the largest specific surface area, allowing for more TiO_2 nanotubes to be grown. As such, more active sites can be provided,

accelerating photoelectrochemical reactions. In the meantime, a proper increase in the mesh density is beneficial for light scattering and absorption, which increases the light utilization. This point can also be confirmed by the comparison in the transmittance of these photoanodes with different mesh densities. An inverse correlation between the mesh density and light transmittance was observed in **Fig. 5b**. When the mesh density was 80 per inch corresponding to a large pore size (about 200 μm), the transmittance was about 53%. As the mesh density increased to 150 corresponding to a pore size of about 80 μm, the transmittance declined to about 42%. With respect to the Ti mesh with a mesh density of 300 per inch and a pore size of about 50 μm, the transmittance was only about 0.15%. The higher transmittance, the smaller absorption. Therefore, when adopting the Ti mesh with a larger mesh density for growing TiO_2 nanotubes, the light utilization becomes higher. In a word, the improvements in the photocatalytic performance with increasing the mesh density of Ti mesh can be mainly attributed to the increased photoelectrochemically active surface area and enhanced light utilization. The photoelectrochemical activities of these photoanodes with different mesh densities were tested a three-electrode system under UV light irradiation in terms of photocurrent response and EIS. As shown in **Fig. 5c**, the photocurrent density increased gradually when increasing the mesh density. The 3D radial TiO_2 nanotubes/Ti mesh photoanodes (80 and 150 per inch) yielded the photocurrent densities of approximately 0.09 and 0.11 mA/cm^2, respectively, while the 3D radial TiO_2 nanotubes/Ti mesh photoanode (300 per inch) exhibited the highest photocurrent density of ~ 0.23 mA/cm^2. Besides, the

TiO_2 nanotubes/Ti mesh photoanode (300 per inch) exhibited the smallest charge transfer resistance (424.5Ω), while it was 670.4Ω for the TiO_2 nanotubes/Ti mesh photoanode (150 per inch) and 1284.0 Ω for the TiO_2 nanotubes/Ti mesh photoanode (80 per inch), as shown in **Fig. 5d**.

These results prove that the Ti mesh with higher mesh density can improve light utilization and provide more active sites, thereby enhancing the photoelectrochemical activity. In addition, these three photoanodes were also assembled into an ordinary PFC to evaluate the performances of electricity generation and pollutant degradation. **Figs. 6a** and **6b** show the *J-V* and *J-P* plots, respectively. The short-circuit current density (J_{SC}), open-circuit voltage (V_{OC}), maximum power density (P_{MAX}) are listed in **Table 1**. As seen, the change of the mesh density of Ti mesh showed ignorable effect on V_{OC}, while the J_{SC} improved gradually when increasing the mesh density, which is consistent with the results on the above photoelectrochemical activities. The reasons have been discussed above. The maximal P_{MAX} of ~ 0.15 mW/cm^2 was then yielded by the PFC with the photoanode prepared by using the Ti mesh (300 per inch), shown in **Fig. 6b** and **Table 1**. Degradation efficiency of MO by the PFCs with these three photoanodes are given in **Fig. 6c**. Similarly, the degradation efficiency increased with the increase of the mesh density. Therefore, the Ti mesh with a larger mesh density is advantageous for developing 3D radial TiO_2 nanotubes/Ti mesh photoanode due to improved light utilization and increased amount of active sites in the present study. However, it should

be pointed out that too large mesh density will significantly resist light transmission inside this type of photoanode, which may cause inefficient utilization of the photoanode at the back side. Selecting the Ti mesh with proper mesh density is critically important for design of such a photoanode.

As mentioned earlier, the light transmittance of the Ti mesh was still relatively high for the Ti meshes with the mesh density of 150 and 80 per inch (**Fig. 5b**), indicating the limited light utilization (Lee et al., 2017b). Meanwhile, the surface area of Ti mesh is still not large enough to further improve the cell performance. To address these two issues, we proposed a stacked 3D radial TiO_2 nanotubes/Ti mesh photoanode by integrating multiple Ti meshes. Here, we chose the Ti mesh with a mesh density of 150 per inch to prepare the stacked photoanode because the Ti mesh with the mesh density of 80 per inch had rather low light utilization and specific surface area for growing TiO_2 nanotubes, and the Ti mesh with a mesh density of 300 per inch had a very small transmittance. We firstly examined the photocatalytic performances of the stacked 3D radial TiO_2 nanotubes/Ti mesh photoanodes with different stacking layer numbers in terms of MO degradation. As shown in **Fig. 7a**, the TiO_2 nanotubes/Ti mesh (two layers) and TiO_2/Ti mesh (three layers) photoanodes displayed enhancement in MO degradation as compared to the TiO_2 nanotubes/Ti mesh (one layer) photoanode, which was in agreement with previous work (Zeng et al., 2020). The MO degradation efficiency appeared to be saturated after stacking two layers. The TiO_2 nanotubes/Ti

mesh (three layers) photoanode exhibited the highest degradation of 96% under UV-light irradiation for 1 h, which was higher than the one-layered photoanode. The enhanced photocatalytic performance can be attributed to two aspects. On one hand, when the Ti meshes were stacked, the total mass of TiO_2 nanotubes increased, providing more active sites and thereby promoting the photocatalytic reactions. On the other hand, stacking multi-layered Ti mesh could enhance the light utilization (Kim et al., 2013). It could be confirmed by the measured transmittance shown in **Fig. 7b**. Under the incident UV light intensity of 5 mW/cm^2, the transmittance was reduced from about 42% (one layer) to about 7% (three layers), implying more protons to be absorbed by stacking three layers. Further increasing the layer number would cause inefficient utilization of the TiO_2 nanotubes/Ti mesh layer at the back side. The light attenuation due to the absorption by the upper layers caused the light intensity in the bottom layer to be reduced. It should be noted that increasing the layer number from two to three, the improvement was not significant as the increase of the layer number from one to two. This might be because more significant light absorption when the layer number increased from one to two (**Fig. 7b**). The Ti mesh structure allowed for efficient light transmission through a single layer because the thickness and mass of the TiO_2 nanotubes were small and less incident photons were absorbed. When the layer number increased to 2, the increased thickness and mass of the TiO_2 nanotubes led more incident photons to be absorbed, which greatly enhanced the light absorption. This point can be confirmed by significant reduction of light transmittance from about 42% (1 layer) to

17% (2 layers). As the layer number further increased to 3, only a small amount of photons could go into the third layer, meaning that much less photons could be absorbed in this layer. Therefore, the improvement in the light absorption was insignificant as the layer number increased from 2 to 3. Except for the photocatalytic degradation performance of the stacked TiO_2 nanotubes/Ti mesh photoanode, the photoelectrochemical performance was also investigated. As shown in **Fig. 7c**, the photocurrent density increased with the increase of the stacking layer number of TiO_2 nanotubes/Ti mesh, and the three-layered TiO_2 nanotubes/Ti mesh photoanode showed an optimized and stable photocurrent density of about 0.19 mA/cm^2 even after five cycles. This is clearly because the increase of the layer number provides more surface area for growing TiO_2 nanotubes, which increases the mass of TiO_2 nanotubes per unit area. Upon illumination, more photo-excited carriers can be generated to enhance the photoelectrochemical reactions. In addition, the Nyquist plots and equivalent circuit shown in **Fig. 7d** revealed that the three-layered TiO_2 nanotubes/Ti mesh photoanode displayed the smallest impedance, indicating low charge transfer resistance (525.9 Ω). The above results indicate that stacking multiple TiO_2 nanotubes/Ti meshes to form stacked 3D radial TiO_2 nanotubes/Ti mesh photoanode is a promising strategy to enhance the photoanode performance because of the increased active surface area and light utilization.

We also tested the performances of the PFC with the stacked 3D radial TiO_2

nanotubes/Ti mesh photoanodes. As shown in **Fig. 8a**, the J_{SC} significantly increased from 0.34 mA/cm^2 to 0.52 mA/cm^2 in response to increasing the stacking layer number from one to three. Meanwhile, the P_{MAX} increased from about 0.12 mW/cm^2 to 0.16 mW/cm^2, presenting an increase by 33% (**Fig. 8b**). Although all the three photoanodes could yield high MO degradation efficiencies in 1 h, the two-layered and three-layered TiO_2 nanotubes/Ti mesh photoanodes showed clear rapid degradation rate (**Fig. 8c**). In 15 minutes, the two-layered and three-layered TiO_2 nanotubes/Ti mesh photoanodes yielded the degradation efficiencies of 65% and 70%, respectively, while the single one only yielded the degradation efficiency of 54%. Correspondingly, the photoelectrochemical reaction rate constant for the three-layered TiO_2 nanotubes/Ti mesh photoanode could be as high as 0.067 ± 0.006 min^{-1}, which was better than the other two photoanodes. In addition, the influence of the initial MO concentration on the degradation efficiency by the PFC with three-layered TiO_2 nanotubes/Ti mesh photoanode was also investigated (**Fig. S8**). In a certain concentration range (10 mg/L to 50 mg/L), a high degradation efficiency could be maintained, demonstrating its applicability in various concentrations. Compared with the data reported listed in **Table 2**, the stacked 3D radial TiO_2 nanotubes/Ti mesh photoanode developed in this study showed better electricity generation and pollutant degradation performance. It is further demonstrated that the use of a stacked photoanode is a promising way to improve performance of the PFC performance.

After examining the performances of the PFCs with different layer numbers, we also tested the dependence of the PFC performance on the pollutant type. Since the three-layered TiO_2 nanotubes/Ti mesh photoanode yielded the best performance, we chose it for studying the effect of the pollutant type on the PFC performance. Here, we compared three typical types of wastewater, including dye contained wastewater (MO) and alcohol contained wastewater (methanol). Meanwhile, it is well known that the wastewater generated by biogas fermentation (biogas slurry) has very complex composition and is difficult to degrade, while it also contains plentiful of chemical energy (Wang et al., 2020a). Hence, the biogas slurry was also chosen to demonstrate the adaptability of the developed PFC. As shown in **Fig. 9a** and **Table 1**, the V_{OC} and J_{SC} in the presence of MO or biogas slurry were lower than methanol. The difference in the PFC performance can be attributed to the molecular structures of pollutants (Li et al., 2013a). Methanol is the simplest alcohol and has no carbon-carbon bond, which can be easily oxidized to release electrons. MO has a more complex molecular structure and contains benzene rings, so that its oxidation is not as easy as methanol. Although the biogas slurry contained a significant amount of organic compounds, the composition is much more complex and usually contains nitrogen, phosphorus, potassium, butyrate, heteroauxin, vitamin, etc (Tan et al., 2016). As a result, the cell performance was the best with methanol, while it was the worst with the biogas slurry. However, even using biogas slurry, J_{SC} and P_{MAX} of 0.44 mA/cm^2 and 0.12 mW/cm^2 were still achieved, as shown in **Fig. 9b**. After running the PFC for 1 h, the chemical

oxygen demand (COD) in the biogas slurry solution was reduced by ~14%, as shown in **Fig. 9c**. These results indicate that the PFC with the developed photoanode can degrade not only those simple organic pollutants but also complex and refractory organic compounds for electricity generation.

The stability of the photoanode is critically important in real applications. As a result, the operation stability of the stacked 3D radial TiO_2 nanotubes/Ti mesh photoanode with three layers was also investigated in the present study. **Fig. 10a** shows the cycling degradation efficiency of MO by the three-layered TiO_2 nanotubes/Ti mesh photoanode. In this testing, the MO solution with a concentration of 10 mg/L and a volume of 2.5 mL was directly poured into the PFC without the discharging and the air-breathing cathode was covered by a carbon plate. After each cycle, the photoanode was washed thoroughly with deionized water, and fresh MO solution was then added. As seen, there was no obvious decrease of degradation efficiency in the tested four cycles, and the developed photoanode exhibited excellent stability. Besides, the long-term discharging performance at a given voltage of 0.3 V was also characterized and the results are given in **Fig. 10b**. Except for a critically high current density at very beginning due to transient effect upon illumination, the discharging current density was relatively stable. After 6-h running, there was almost no significant decline in the current density, demonstrating good stability of the developed photoanode.

4 Conclusions

Growth of the TiO_2 nanotubes on the planar substrates to serve as the photoanode for photocatalytic fuel cells usually suffers from low specific surface area and light utilization. In this work, therefore, a 3D radial TiO_2 nanotubes/Ti mesh photoanode was developed by electrochemical anodization method, and applied to a photocatalytic fuel cell. Compared with planar photoanode, the specific surface area and electrochemical active sites of the proposed 3D photoanode were increased. Moreover, the highly-ordered TiO_2 nanotubes could enhance the electron transfer and inhibit the recombination of photo-excited carriers represented by small charge transfer impedance. Because of these merits, the current density J_{SC} and maximum power density P_{MAX} of the proposed photoanode reached 0.23 mA/cm^2 and 0.074 mW/cm^2 in the staggered PFC using the Ti mesh with a mesh density of 300 per inch, respectively, which was better than the TiO_2 nanotubes/Ti foil and TiO_2 nanoparticles/Ti mesh photoanodes. When the mesh density increased from 80 to 300 per inch, the J_{SC} and P_{MAX} for the ordinary PFC raised to 0.49 mA/cm^2 and 0.15 mW/cm^2 due to the improved specific surface area for growing TiO_2 nanotubes and enhanced light utilization. More importantly, the use of Ti mesh as a substrate makes it easy to integrate multiple TiO_2 nanotubes/Ti meshes to form stacked 3D radial TiO_2 nanotubes/Ti mesh photoanode. As compared to the single-layered TiO_2 nanotubes/Ti mesh (150 per inch) photoanode, the J_{SC} could be increased to 0.52 mA/cm^2 by the three-layered TiO_2 nanotubes/Ti mesh photoanode. The photoanode with the stacked design solve the problem of low light

utilization when using the Ti mesh with relatively small mesh density. The feasibility of the stacked photoanode was also assessed in terms of its adaptability to various organic compounds. The highest degradation efficiency of 98% and power density of 0.16 mW/cm^2 as well as excellent stability were achieved. In summary, the use of Ti mesh as a substrate for growing TiO_2 nanotubes to serve as a photoanode provides a promising strategy to develop a high-performance 3D-designed photoanode for the PFC applications, which can also be applied in other photoelectrochemical systems.

Acknowledgments

The authors gratefully acknowledge the financial supports of the National Natural Science Foundation of China (No. 51925601 and No. 52161160333), Innovative Research Group Project of National Natural Science Foundation of China (No. 52021004) and Research Grants Council of the Hong Kong Special Administrative Region, China (No. N_PolyU559/21).

Supplementary Materials

Supplementary Fig. S1-S8

Reference

Bai, J., Wang, R., Li, Y., Tang, Y., Zeng, Q., Xia, L., Li, X., Li, J., Li, C., Zhou, B., 2016. A solar light driven dual photoelectrode photocatalytic fuel cell (PFC) for simultaneous wastewater treatment and electricity generation. J. Hazard. Mater. 311, 51-62. https://doi.org/10.1016/j.jhazmat.2016.02.052

Bao, R., Geng, J., Sullivan, J. A., Xia, J., Wang, W., Wong, W.-Y., Li, H., 2018. Hierarchical 3D TiO_2 nanotube arrays sensitized by graphene oxide and Zn_xCd_yS for high performance photoelectrochemical applications. Phys. Status Solidi A. 215(24), 1800436. https://doi.org/10.1002/pssa.201800436

Barbosa, M. O., Moreira, N. F. F., Ribeiro, A. R., Pereira, M. F. R., Silva, A. M. T., 2016. Occurrence and removal of organic micropollutants: An overview of the watch list of EU Decision 2015/495. Water Res. 94, 257-279. https://doi.org/10.1016/j.watres.2016.02.047

Chen, D., Cheng, Y., Zhou, N., Chen, P., Wang, Y., Li, K., Huo, S., Cheng, P., Peng, P., Zhang, R., Wang, L., Liu, H., Liu, Y., Ruan, R., 2020a. Photocatalytic degradation of organic pollutants using TiO_2-based photocatalysts: A review. J. Clean Prod. 268. https://doi.org/10.1016/j.jclepro.2020.121725

Chen, X., Yao, J., Xia, B., Gan, J., Gao, N., Zhang, Z., 2020b. Influence of pH and DO on the ofloxacin degradation in water by UVA-LED/TiO_2 nanotube arrays photocatalytic fuel cell: mechanism, ROSs contribution and power generation. J. Hazard. Mater. 383, 121220. https://doi.org/10.1016/j.jhazmat.2019.121220

Delavari, S., Amin, N. A. S., 2016. Photocatalytic conversion of CO_2 and CH_4 over immobilized titania nanoparticles coated on mesh: Optimization and kinetic study. Appl. Energy. 162, 1171-1185. https://doi.org/10.1016/j.apenergy.2015.03.125

He, X., Chen, M., Chen, R., Zhu, X., Liao, Q., Ye, D., Zhang, B., Zhang, W., Yu, Y., 2018. A solar responsive photocatalytic fuel cell with the membrane electrode assembly design for simultaneous wastewater treatment and electricity generation. J. Hazard. Mater. 358, 346-354. https://doi.org/10.1016/j.jhazmat.2018.07.031

He, Y., Yuan, R., Yan, J., Li, J., 2021. A highly efficient NiFe-layer double hydroxide/TiO_2 heterojunction photoanode-based high-performance bifunctional photocatalytic fuel cell. Mater. Today Commun. 26. https://doi.org/10.1016/j.mtcomm.2021.102177

Hu, X., Zhang, T., Jin, Z., Zhang, J., Xu, W., Yan, J., Zhang, J., Zhang, L., Wu, Y., 2008. Fabrication of carbon-modified TiO_2 nanotube arrays and their photocatalytic activity. Mater. Lett. 62(30), 4579-4581. https://doi.org/10.1016/j.matlet.2008.08.051

Kim, H., Khamwannah, J., Choi, C., Shi, Y., Jin, S., 2013. Hydrothermally grown TiO_2 nanotubes on multi-layered Ti mesh electrodes for enhanced photoelectrochemical reaction. MRS Commun. 3(4), 235-240. https://doi.org/10.1557/mrc.2013.38

Lashkov, A. V., Fedorov, F. S., Vasilkov, M. Y., Kochetkov, A. V., Belyaev, I. V., Plugin, I. A., Varezhnikov, A. S., Filipenko, A. N., Romanov, S. A., Nasibulin, A. G., 2020. The Ti wire functionalized with inherent TiO_2 nanotubes by anodization as one-electrode gas sensor: A proof-of-concept study. Sens. Actuators B. 306. https://doi.org/10.1016/j.snb.2019.127615

Lee, S. L., Ho, L. N., Ong, S. A., Wong, Y. S., Voon, C. H., Khalik, W. F., Yusoff, N. A., Nordin, N., 2017a. A highly efficient immobilized ZnO/Zn photoanode for degradation of azo dye Reactive Green 19 in a photocatalytic fuel cell. Chemosphere. 166, 118-125. https://doi.org/10.1016/j.chemosphere.2016.09.082

Lee, W. C., Fang, Y., Commandeur, D., Qian, R., Al-Abdullah, Z. T., Chen, Q., 2017b. Ultra rapid direct heating synthesis of ZnO nanorods with improved light trapping from stacked photoanodes for high efficiency photocatalytic water splitting. Nanotechnology. 28(35), 355402. https://doi.org/10.1088/1361-6528/aa7c7c

Li, J., Li, J., Chen, Q., Bai, J., Zhou, B., 2013a. Converting hazardous organics into clean energy using a solar responsive dual photoelectrode photocatalytic fuel cell. J. Hazard. Mater. 262, 304-310. https://doi.org/10.1016/j.jhazmat.2013.08.066

Li, K., Xu, Y., He, Y., Yang, C., Wang, Y., Jia, J., 2013b. Photocatalytic fuel cell (PFC) and dye self-photosensitization photocatalytic fuel cell (DSPFC) with BiOCl/Ti photoanode under UV and visible light irradiation. Environ. Sci. Technol. 47(7), 3490-3497. https://doi.org/10.1021/es303968n

Li, K., Zhang, H., Tang, T., Xu, Y., Ying, D., Wang, Y., Jia, J., 2014. Optimization and application of TiO_2/Ti-Pt photo fuel cell (PFC) to effectively generate electricity and degrade organic pollutants simultaneously. Water Res. 62, 1-10. https://doi.org/10.1016/j.watres.2014.05.044

Li, W. W., Yu, H. Q., Rittmann, B. E., 2015. Chemistry: Reuse water pollutants. Nature. 528(7580), 29-31. https://doi.org/10.1038/528029a

Liao, J., Lin, S., Zhang, L., Pan, N., Cao, X., Li, J., 2012. Photocatalytic degradation of methyl orange using a TiO_2/Ti mesh electrode with 3D nanotube arrays. ACS Appl. Mater. Interfaces. 4(1), 171-177. https://doi.org/10.1021/am201220e

Lin, Y., Feng, H., Chen, R., Zhang, B., An, L., 2020. One-dimensional TiO_2 nanotube array photoanode for a microfluidic all-vanadium photoelectrochemical cell for solar energy storage. Catal. Sci. Technol. 10(13), 4352-4361. https://doi.org/10.1039/d0cy00342e

Liu, Y., Zhou, B., Li, J., Gan, X., Bai, J., Cai, W., 2009a. Preparation of short, robust and highly ordered TiO_2 nanotube arrays and their applications as electrode. Appl Catal B. 92(3-4), 326-332. https://doi.org/10.1016/j.apcatb.2009.08.011

Liu, Z., Subramania, V., Misra, M., 2009b. Vertically oriented TiO_2 nanotube arrays grown on Ti meshes for flexible dye-sensitized solar cells. J. Phys. Chem. C. 113(31), 14028-14033. https://doi.org/10.1021/jp903342s

Liu, Z., Zhang, Q., Zhao, T., Zhai, J., Jiang, L., 2011. 3-D vertical arrays of TiO_2 nanotubes on Ti meshes: Efficient photoanodes for water photoelectrolysis. J. Mater. Chem. 21(28), 10354-10358. https://doi.org/10.1039/c1jm11072a

Liu, Z., Zhang, X., Nishimoto, S., Jin, M., Tryk, D. A., Murakami, T., Fujishima, A., 2008. Highly ordered TiO_2 nanotube arrays with controllable length for photoelectrocatalytic degradation of phenol. J. Phys. Chem. C. 112(1), 253-259. https://doi.org/10.1021/jp0772732

Luo, D., Liu, B., Fujishima, A., Nakata, K., 2019. TiO_2 nanotube arrays formed on Ti meshes with periodically arranged holes for flexible dye-sensitized solar cells. ACS Appl. Nano Mater. 2(6), 3943-3950. https://doi.org/10.1021/acsanm.9b00849

Martin, M., Leonid, S., Tomáš, R., Jan, Š., Jaroslav, K., Mariana, K., Michaela, J., František, P., Gustav, P., 2017. Anatase TiO_2 nanotube arrays and titania films on titanium mesh for photocatalytic NO_X removal and water cleaning. Catal. Today. 287, 59-64. https://doi.org/10.1016/j.cattod.2016.10.011

O'Shea, K. E., Pernas, E., Saiers, J., 1999. The influence of mineralization products on the coagulation of TiO_2 photocatalyst. Langmuir. 15(6), 2071-2076. https://doi.org/10.1021/la9806808

Ocampo, R. A., Echeverria, F. E., 2021. TiO_2 nanotubes produced on curved titanium surfaces using aqueous electrolytes with carboxymethyl cellulose. Physica E. 125. https://doi.org/10.1016/j.physe.2020.114391

Pan, D., Xiao, S., Chen, X., Li, R., Cao, Y., Zhang, D., Pu, S., Li, Z., Li, G., Li, H., 2019. Efficient photocatalytic fuel cell via simultaneous visible-photoelectrocatalytic degradation and electricity generation on a porous coral-like WO_3/W photoelectrode. Environ. Sci. Technol. 53(7), 3697-3706. https://doi.org/10.1021/acs.est.8b05685

Qiu, L., Wang, Q., Liu, Z., Zhao, Q., Tian, X., Li, H., Gao, S., 2018. Preparation of 3D TiO_2 nanotube arrays photoelectrode on Ti mesh for photoelectric conversion and

photoelectrocatalytic removal of pollutant. Sep. Purif. Technol. 207, 206-212. https://doi.org/10.1016/j.seppur.2018.06.050

Sankapal, B., Lux-Steiner, M. C., Ennaoui, A., 2005. Synthesis and characterization of anatase-TiO_2 thin films. Appl. Surf. Sci. 239(2), 165-170. https://doi.org/10.1016/j.apsusc.2004.05.142

Saravanan, A., Senthil Kumar, P., Jeevanantham, S., Karishma, S., Tajsabreen, B., Yaashikaa, P. R., Reshma, B., 2021. Effective water/wastewater treatment methodologies for toxic pollutants removal: Processes and applications towards sustainable development. Chemosphere. 280, 130595. https://doi.org/10.1016/j.chemosphere.2021.130595

Sivalingam, G., Nagaveni, K., Hegde, M., Madras, G., 2003. Photocatalytic degradation of various dyes by combustion synthesized nano anatase TiO_2. Appl Catal B. 45(1), 23-38. https://doi.org/10.1016/s0926-3373(03)00124-3

Sopha, H., Kashimbetova, A., Hromadko, L., Saldan, I., Celko, L., Montufar, E. B., Macak, J. M., 2021. Anodic TiO_2 nanotubes on 3D-printed titanium meshes for photocatalytic applications. Nano Lett. 21(20), 8701-8706. https://doi.org/10.1021/acs.nanolett.1c02815

Tan, F., Wang, Z., Zhouyang, S., Li, H., Xie, Y., Wang, Y., Zheng, Y., Li, Q., 2016. Nitrogen and phosphorus removal coupled with carbohydrate production by five microalgae cultures cultivated in biogas slurry. Bioresour Technol. 221, 385-393. https://doi.org/10.1016/j.biortech.2016.09.030

Tauc, J., Grigorovici, R., Vancu, A., 1966. Optical properties and electronic structure of amorphous germanium. Phys. Status Solidi B. 15(2), 627-637. https://doi.org/10.1002/pssb.19660150224

Wang, P., Zhang, X., Gouda, S. G., Yuan, Q., 2020a. Humidification-dehumidification process used for the concentration and nutrient recovery of biogas slurry. J. Clean Prod. 247. https://doi.org/10.1016/j.jclepro.2019.119142

Wang, X., Sun, M., Murugananthan, M., Zhang, Y., Zhang, L., 2020b. Electrochemically self-doped WO_3/TiO_2 nanotubes for photocatalytic degradation of volatile organic compounds. Appl Catal B. 260, 118205. https://doi.org/10.1016/j.apcatb.2019.118205

Yang, Y., Albu, SP., Kim, D., Schmuki, P., 2011, Enabling the anodic growth of highly ordered V_2O_5 nanoporous/nanotubular structures. Angew. Chem. Int. Edit. 50(39),

9071-9075. https://doi.org/ 10.1002/anie.201104029

Ye, Y., Bruning, H., Li, X., Yntema, D., Rijnaarts, H. H. M., 2018. Significant enhancement of micropollutant photocatalytic degradation using a TiO_2 nanotube array photoanode based photocatalytic fuel cell. Chem. Eng. J. 354, 553-562. https://doi.org/10.1016/j.cej.2018.08.064

Zeng, Q., Bai, J., Li, J., Li, L., Xia, L., Zhou, B., Sun, Y., 2018. Highly-stable and efficient photocatalytic fuel cell based on an epitaxial $TiO_2/WO_3/W$ nanothorn photoanode and enhanced radical reactions for simultaneous electricity production and wastewater treatment. Appl. Energy. 220, 127-137. https://doi.org/10.1016/j.apenergy.2018.03.042

Zeng, Q., Chang, S., Beyhaqi, A., Wang, M., Hu, C., 2020. Efficient electricity production coupled with water treatment via a highly adaptable, successive water-energy synergistic system. Nano Energy. 67. https://doi.org/10.1016/j.nanoen.2019.104237

Zhao, K., Zeng, Q., Bai, J., Li, J., Xia, L., Chen, S., Zhou, B., 2017. Enhanced organic pollutants degradation and electricity production simultaneously via strengthening the radicals reaction in a novel Fenton-photocatalytic fuel cell system. Water Res. 108, 293-300. https://doi.org/10.1016/j.watres.2016.11.002

Zhu, K., Vinzant, T. B., Neale, N. R., Frank, A. J., 2007. Removing structural disorder from oriented TiO_2 nanotube arrays: reducing the dimensionality of transport and recombination in dye-sensitized solar cells. Nano Lett. 7(12), 3739-3746. https://doi.org/10.1021/nl072145a

List of Table

Table 1 Performances of PFCs with various photoanodes

Photoanode	Pollutant	PFC design	J_{SC} (mA/cm^2)	V_{OC} (V)	P_{MAX} (mW/cm^2)	Removal efficiency (%)
TiO_2 nanotubes/Ti mesh (300 per inch)	MO	ordinary	0.49	0.85	0.15	96±0.7
TiO_2 nanotubes/Ti mesh (300 per inch)	MO	staggered	0.23	0.81	0.074	88±5.2
TiO_2 nanotubes/Ti foil	MO	staggered	0.15	0.82	0.045	56±0.1
TiO_2 nanoparticles/Ti mesh (300 per inch)	MO	staggered	0.062	0.61	0.012	73±0.02
TiO_2 nanotubes/Ti mesh (80 per inch)	MO	ordinary	0.28	0.87	0.10	80±3.0
TiO_2 nanotubes/Ti mesh (150 per inch)	MO	ordinary	0.34	0.91	0.12	96±2.5
TiO_2 nanotubes/Ti mesh (150 per inch) (two layers)	MO	ordinary	0.52	0.91	0.15	97±1.6
TiO_2 nanotubes/Ti mesh (150 per inch) (three layers)	MO	ordinary	0.52	0.91	0.16	98±0.7
TiO_2 nanotubes/Ti mesh (150 per inch) (three layers)	Methanol	ordinary	0.55	1.07	0.20	-
TiO_2 nanotubes/Ti mesh (150 per inch) (three layers)	Biogas slurry	ordinary	0.44	0.73	0.12	14

3

Table 2 PFC performance comparison

Configuration	Light source	Pollutant	J_{SC} (mA/cm^2)	V_{OC} (V)	P_{MAX} (mW/cm^2)	Refs.
TiO_2 nanotubes/Ti sheet + Cu_2O nanowires/Cu	Xenon lamp	MO (20 mg/L)	0.17	0.64	0.027	(Li, J. et al., 2013)
ZnO/Zn + Pt/C	UV light	RG19 (10 mg/L)	0.022	0.94	0.0053	(Lee et al., 2017a)
TiO_2/Ti + Pt/Ti	UV light	RBR (20 mg/L)	0.81	0.06	0.015	(Li et al., 2014)
TiO_2 nanotubes/Ti foil + Cu	UV light	MCPA (1 mg/L)	0.028	0.12	-	(Ye et al., 2018)
CdS-ZnS-TiO_2 + Pt/C	Xenon lamp	10% ethanol	2.1	1.07	1.01	(He et al., 2018)
TiO_2/WO_3/W + Pt/BJS	Xenon lamp	Atrazine (10 mg/L)	0.37	0.76	0.56	(Zeng et al., 2018)
$BiVO_4$/TiO_2 nanotubes + ZnO/CuO nanowires	Xenon lamp	MO (20 mg/L)	0.35	0.61	0.077	(Bai et al., 2016)
NiFe-LDH/TiO_2 + Cu_2O/Cu	Xenon lamp	MO (10 mg/L)	0.40	0.74	0.12	(He et al., 2021)
BiOCl/Ti + Pt/Ti	mercury lamp UV light	RhB (10 mg/L)	0.012	0.66	0.0030	(Li, K. et al., 2013)
WO_3/W + Pt	Xenon lamp	MO (5 mg/L)	0.028	0.51	0.003	(Pan et al., 2019)
TiO_2 nanotubes + Pt	UVA-LEDs	OFX (1 mg/L)	0.70	1.35	0.13	(Chen et al., 2020b)

TiO_2 nanotubes/Ti mesh (three layers) + Pt/C	UV light	MO (10 mg/L)	0.52	0.91	0.16	This work

4

Figure Captions

Fig. 1 Constructions of (a) staggered PFC and (b) ordinary PFC.

Fig. 2 SEM images of 3D radial TiO_2 nanotubes/Ti mesh photoanode: (a) Top view and (b) the cross-sectional view; (c) N_2 adsorption/desorption isotherms of various photoanodes; (d) TEM image of 3D radial TiO_2 nanotubes/Ti mesh photoanode; (e) XRD pattern and (f) UV−vis DRS spectra and corresponding band gap.

Fig. 3 (a) Degradation efficiencies of various photoanodes, (b) apparent photocatalytic reaction rate constants, (c) photocurrent responses and (d) Nyquist plots of various photoanodes and equivalent circuit.

Fig. 4 Comparisons in (a) discharging performance, (b) power density and (c) degradation efficiency by PFCs with various photoanodes.

Fig. 5 Effect of the mesh density of Ti mesh: (a) Degradation efficiency, (b) Light transmittance (c) Photocurrent response and (d) Nyquist plots of various photoanodes and equivalent circuit.

Fig. 6 Effect of the mesh density of Ti mesh: (a) Discharging curves, (b) Power density curves and (c) Degradation efficiencies under the PFC operation mode.

Fig. 7 Dependence of stacked 3D radial TiO_2 nanotubes/Ti mesh photoanode performance on layer number: (a) Degradation efficiency, (b) Transmittance, (c) Photocurrent response and (d) EIS Nyquist plots of various photoanodes and equivalent circuit.

Fig. 8 Performances of the PFC with stacked 3D radial TiO_2 nanotubes/Ti mesh photoanode: (a) Discharging curves, (b) Power density curves and (c) Degradation efficiencies.

Fig. 9 Applicability of the developed PFC to various pollutants: (a) Discharging curves; (b) Power density curves; (c) Variation of COD in the presence of biogas slurry.

Fig. 10 Stability of the developed photoanode: (a) Cycling photocatalytic degradation efficiency of MO; (b) Long-term discharging current density at a given voltage.

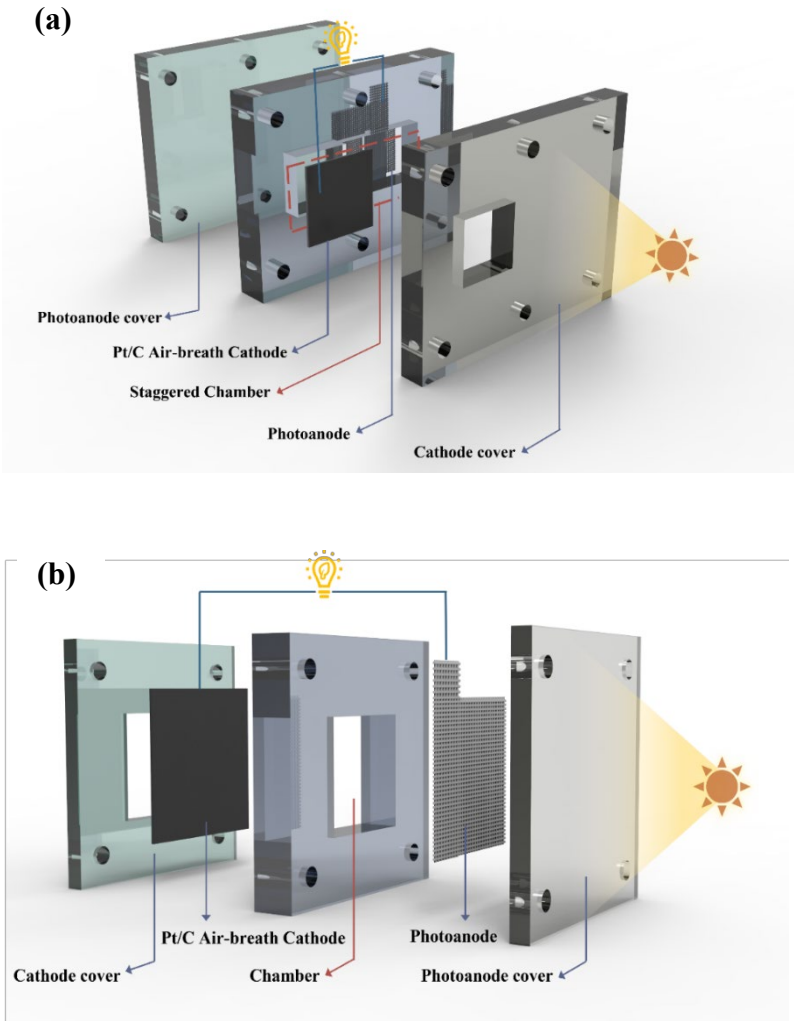

Fig. 1 Constructions of (a) staggered PFC and (b) ordinary PFC.

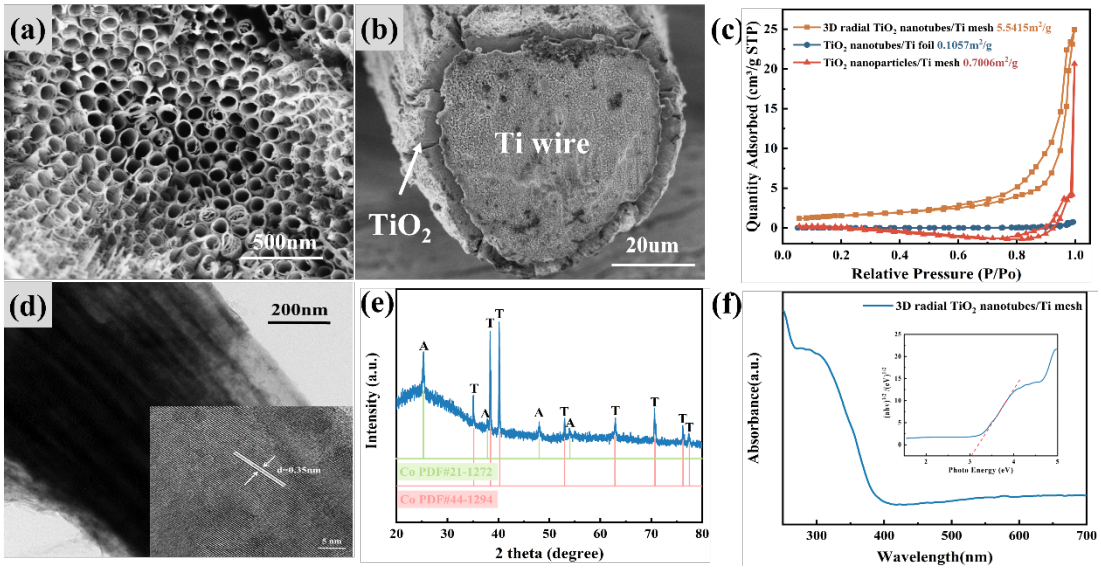

Fig. 2 SEM images of 3D radial TiO_2 nanotubes/Ti mesh photoanode: (a) Top view and (b) the cross-sectional view; (c) N_2 adsorption/desorption isotherms of various photoanodes; (d) TEM image of 3D radial TiO_2 nanotubes/Ti mesh photoanode; (e) XRD pattern and (f) UV−vis DRS spectra and corresponding band gap.

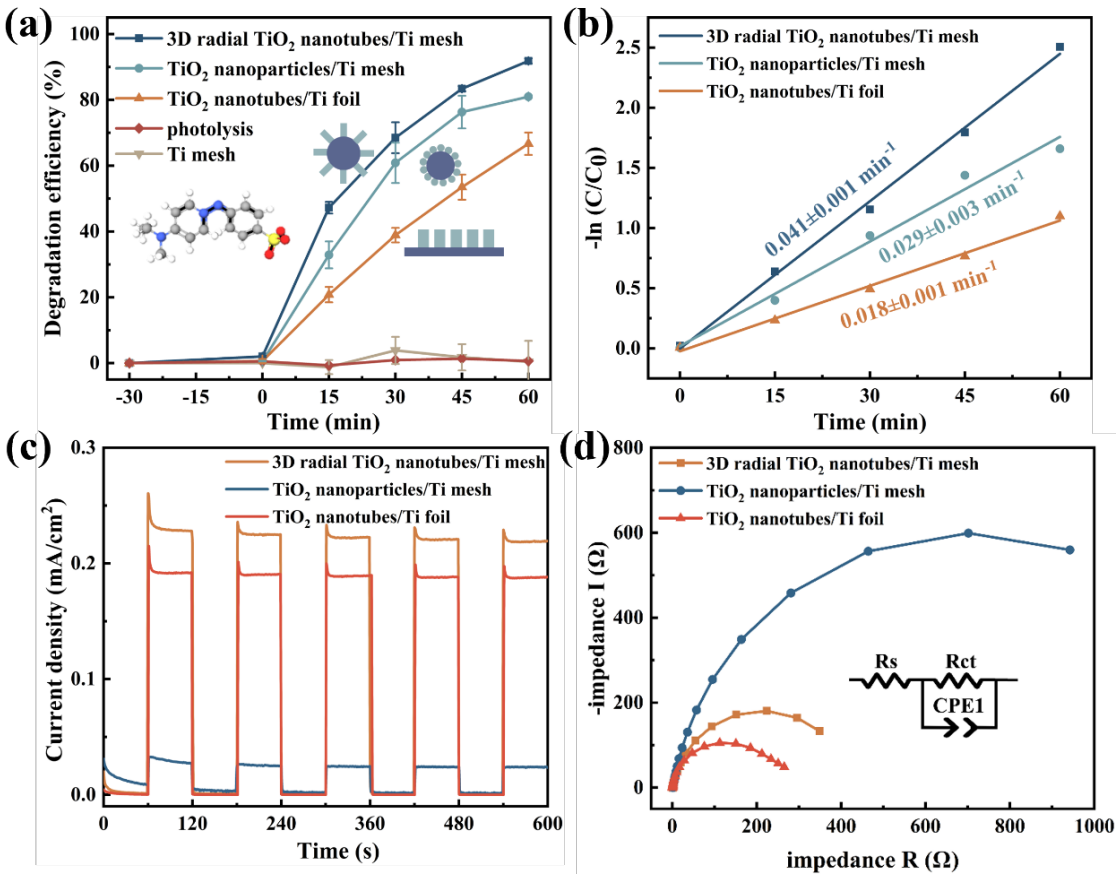

Fig. 3 (a) Degradation efficiencies of various photoanodes, (b) apparent photocatalytic reaction rate constants, (c) photocurrent responses and (d) Nyquist plots of various photoanodes and equivalent circuit.

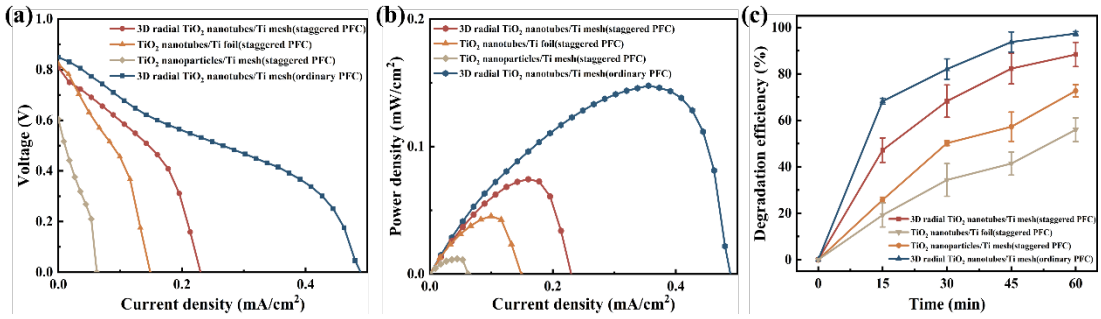

Fig. 4 Comparisons in (a) discharging performance, (b) power density and (c) degradation efficiency by PFCs with various photoanodes.

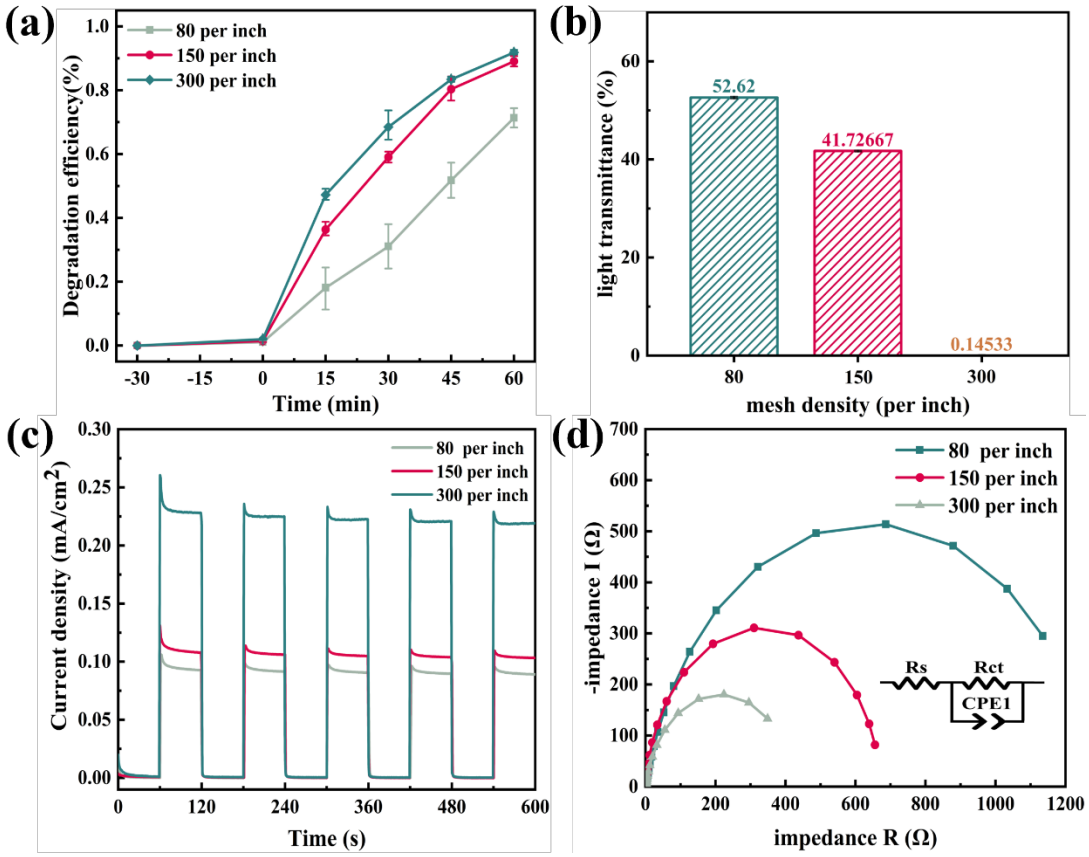

Fig. 5 Effect of the mesh density of Ti mesh: (a) Degradation efficiency, (b) Light transmittance (c) Photocurrent response and (d) Nyquist plots of various photoanodes and equivalent circuit.

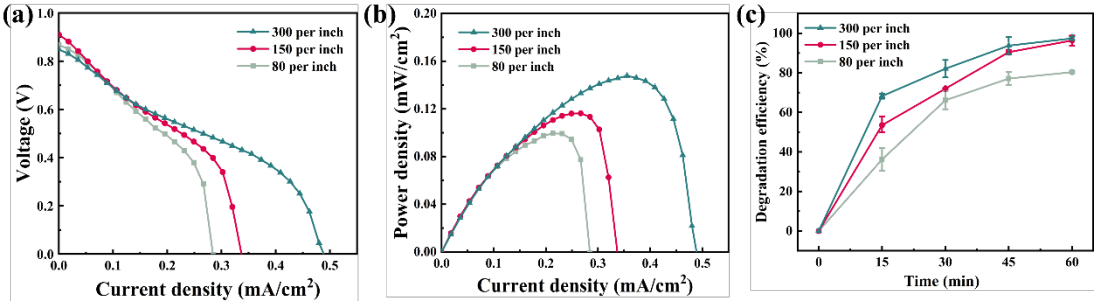

Fig. 6 Effect of the mesh density of Ti mesh: (a) Discharging curves, (b) Power density curves and (c) Degradation efficiencies under the PFC operation mode.

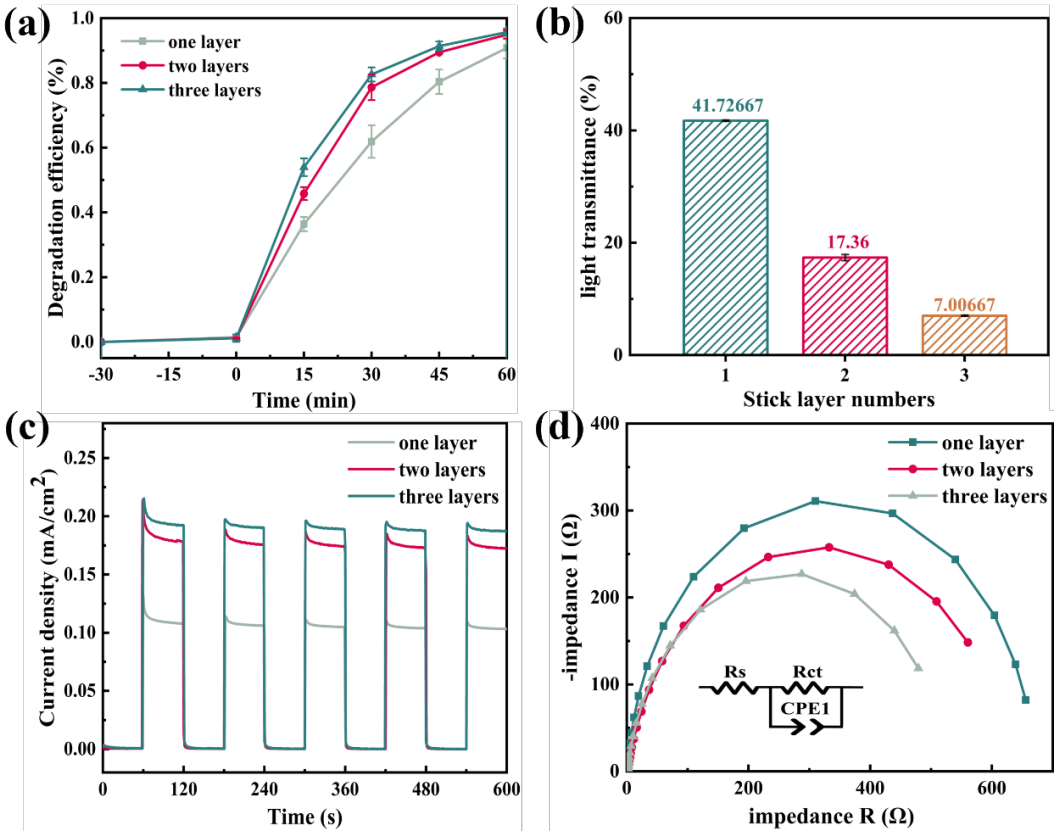

Fig. 7 Dependence of stacked 3D radial TiO_2 nanotubes/Ti mesh photoanode performance on layer number: (a) Degradation efficiency, (b) Transmittance, (c) Photocurrent response and (d) Nyquist plots of various photoanodes and equivalent circuit.

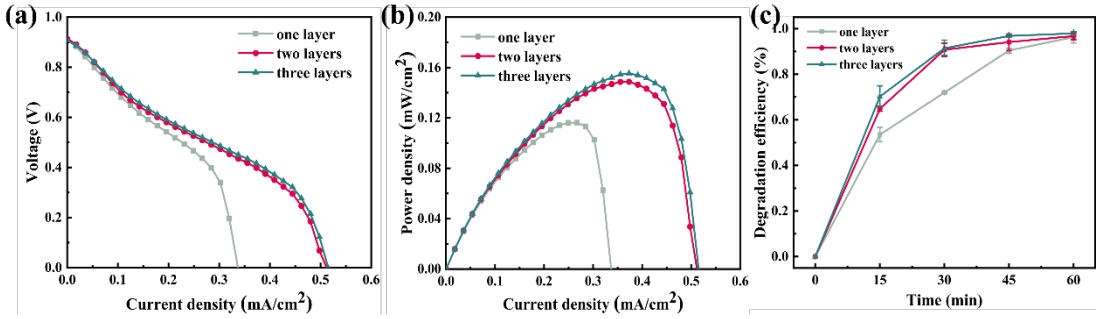

Fig. 8 Performances of the PFC with the stacked 3D radial TiO_2 nanotubes/Ti mesh photoanode: (a) Discharging curves, (b) Power density curves and (c) Degradation efficiencies.

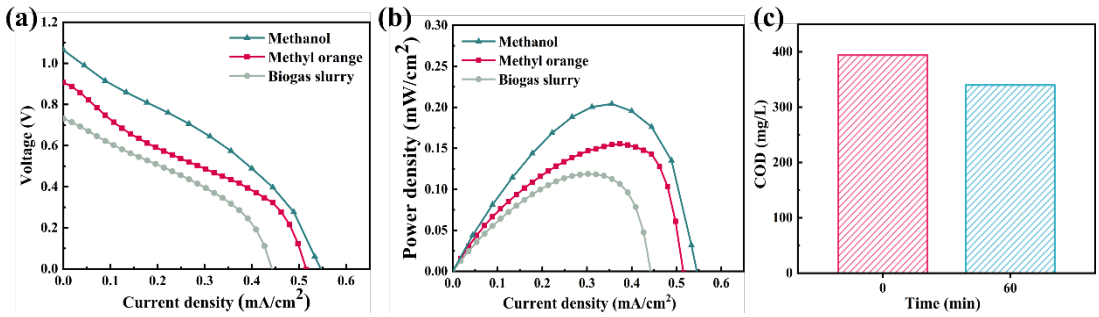

Fig. 9 Applicability of the developed PFC to various pollutants: (a) Discharging curves; (b) Power density curves; (c) Variation of COD in the presence of biogas slurry (KOH: 1.0 M; Light intensity: 5 mW/cm^2; Methanol concentration: 1.0 M; MO concentration: 10 mg/L; Biogas slurry: 100%).

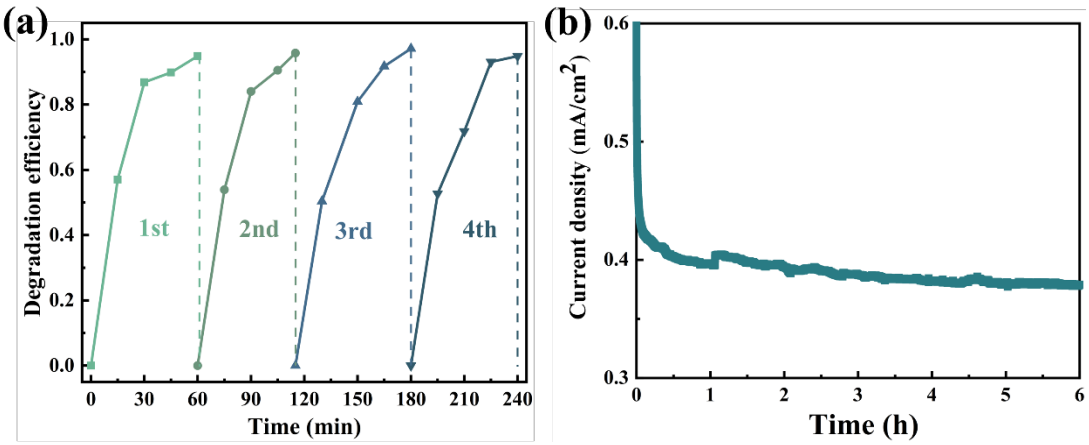

Fig. 10 Stability of the developed photoanode: (a) Cycling photocatalytic degradation efficiency of MO; (b) Long-term discharging current density at a given voltage.

Supplementary Materials for

3D radially-grown TiO_2 nanotubes/Ti mesh photoanode for photocatalytic fuel cells towards simultaneous wastewater treatment and electricity generation

Yuxin Liu [a,b], Rong Chen [a,b]*, Xun Zhu [a,b], Dingding Ye [a,b], Yang Yang [a,b], Jinwang Li [a,b], Dechao Wang [a,b], Liang An [c], Qiang Liao [a,b]

[a] Key Laboratory of Low-grade Energy Utilization Technologies and Systems (Chongqing University), Ministry of Education, Chongqing 400030, China

[b] Institute of Engineering Thermophysics, School of Energy and Power Engineering, Chongqing University, Chongqing 400030, China

[c] Department of Mechanical Engineering, The Hong Kong Polytechnic University, Hung Hom, Kowloon, Hong Kong, China

* Corresponding author

[a,b] Tel.: 0086-23-65102019; fax: 0086-23-65102474; e-mail: rchen@cqu.edu.cn (Rong Chen)

Supplementary Fig. S1-S8

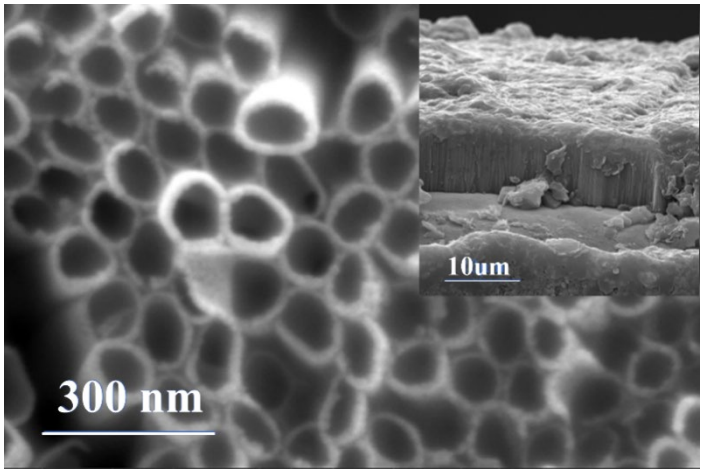

Fig. S1 SEM image of TiO_2 nanotubes/Ti foil.

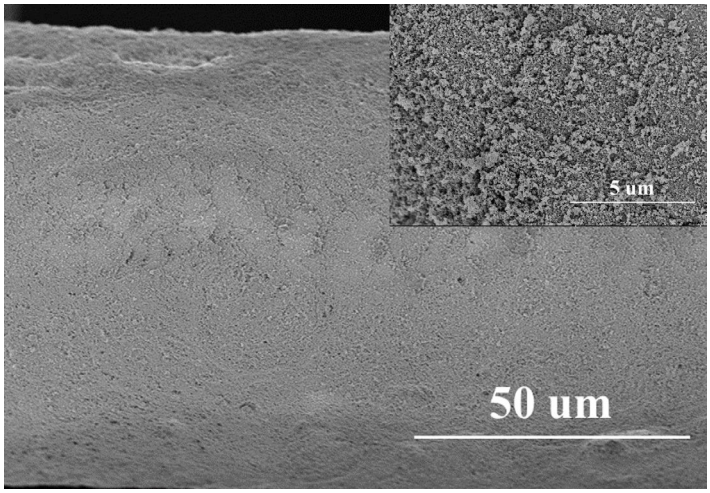

Fig. S2 SEM image of TiO_2 nanoparticles/Ti mesh.

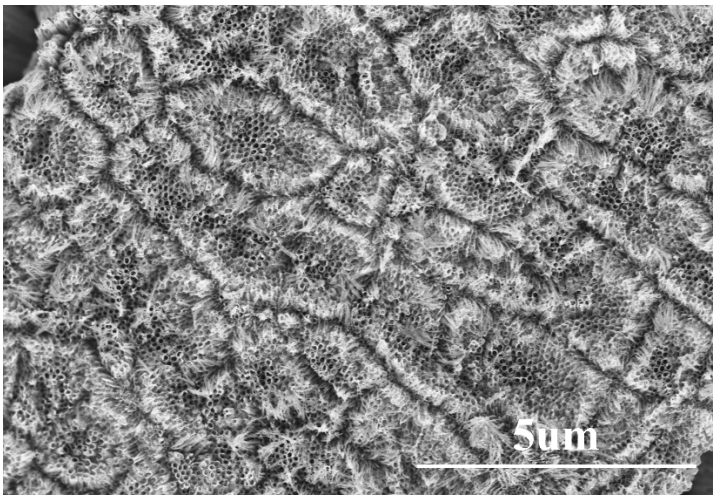

Fig. S3 Top-view SEM images of the 3D radial TiO_2 nanotubes/Ti mesh.

In this work, the mass of TiO_2 nanotubes grown on Ti mesh could be achieved by:

$$M = \rho V \quad (1)$$

where M (mg/cm^2) is the mass of TiO_2 nanotubes; ρ is the density of anatase TiO_2; V (cm^3) is the total volume of the prepared TiO_2 nanotubes/Ti mesh, which could be estimated by:

$$V = nLSA \quad (2)$$

$$n = \frac{10^{14}}{\sqrt{3}Do^2} \quad (3)$$

$$S = \frac{\pi(Do^2 - Di^2)}{4\times10^{14}} \quad (4)$$

where *Di* (nm) and *Do* (nm) denote the average inner and outer diameter of the nanotubes; n (nanotubes per cm^2) is the nanotube density; *L* (nm) is the mean tube length of the TiO_2 nanotubes; *S* (cm^2) is the top area of a single nanotube; *A* is the photoanode area. For the Ti foil, A= 1.5 × 1.5 =2.25 cm^2, but for the Ti mesh with 150 per inch, A= 1.5 × 1.5 × (1-$80^2/140^2$) =1.52 cm^2.

Table S1 Parameters of TiO_2 nanotubes grown on different substrates.

Photoanode	***Do*** **(nm)**	***Di*** **(nm)**	***L*** **(μm)**	***M*** **(mg/cm^2)**
3D radical TiO_2 nanotubes/Ti mesh	109	84	6.7	0.60
TiO_2 nanotubes/Ti foil	104	85	8.8	0.97

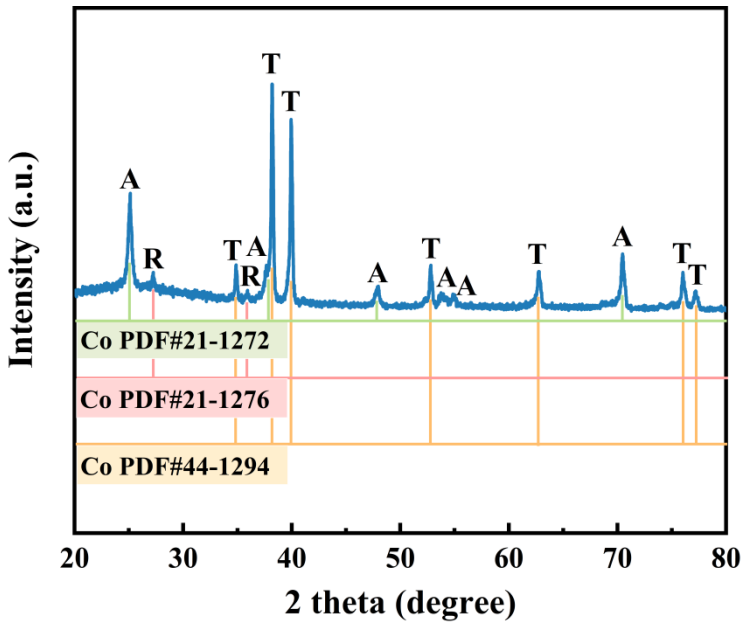

Fig. S4 XRD pattern of TiO_2 nanoparticles/Ti mesh.

Table S2 Charge transfer resistances of various photoanodes

Photoanode	Rct (Ω)
TiO_2 nanotubes/Ti mesh (300 per inch)	424.5±25.0
TiO_2 nanoparticles/Ti mesh (300 per inch)	1412.0±42.2
TiO_2 nanotubes/Ti foil	548.4±9.6
TiO_2 nanotubes/Ti mesh (80 per inch)	1284.0±46.6
TiO_2 nanotubes/Ti mesh (150 per inch)	670.4±19.9
TiO_2 nanotubes/Ti mesh (150 per inch) (two layers)	632.9±22.4
TiO_2 nanotubes/Ti mesh (150 per inch) (three layers)	525.9±20.0

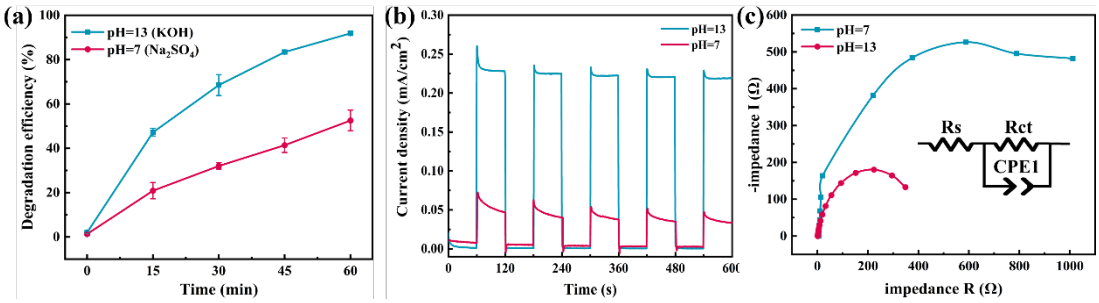

150

151 **Fig. S5** Effect of pH value: (a) Degradation efficiency, (b) Photocurrent response and

152 (c) EIS results.

153

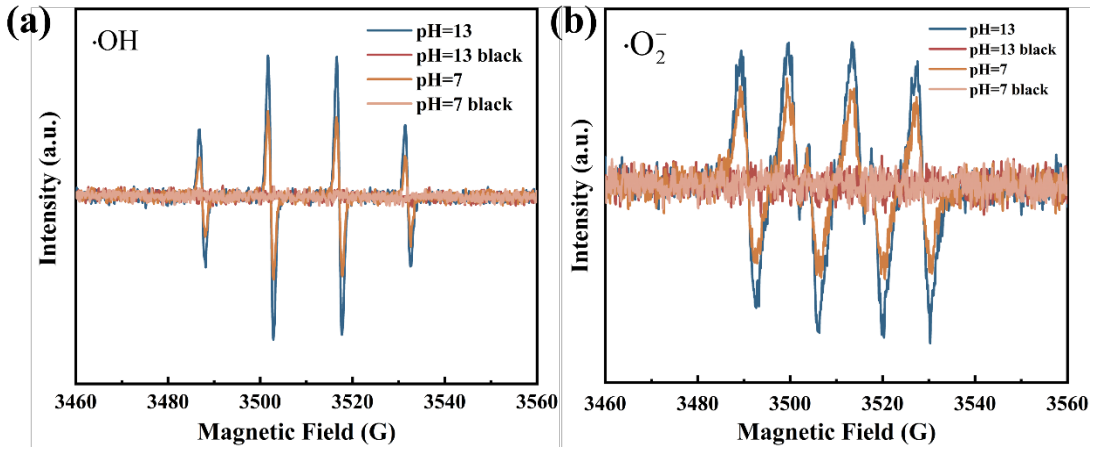

154

155 **Fig. S6** EPR spectra of 3D radially-grown TiO_2 nanotubes/Ti mesh photoanode under

156 alkaline and neutral conditions.

157

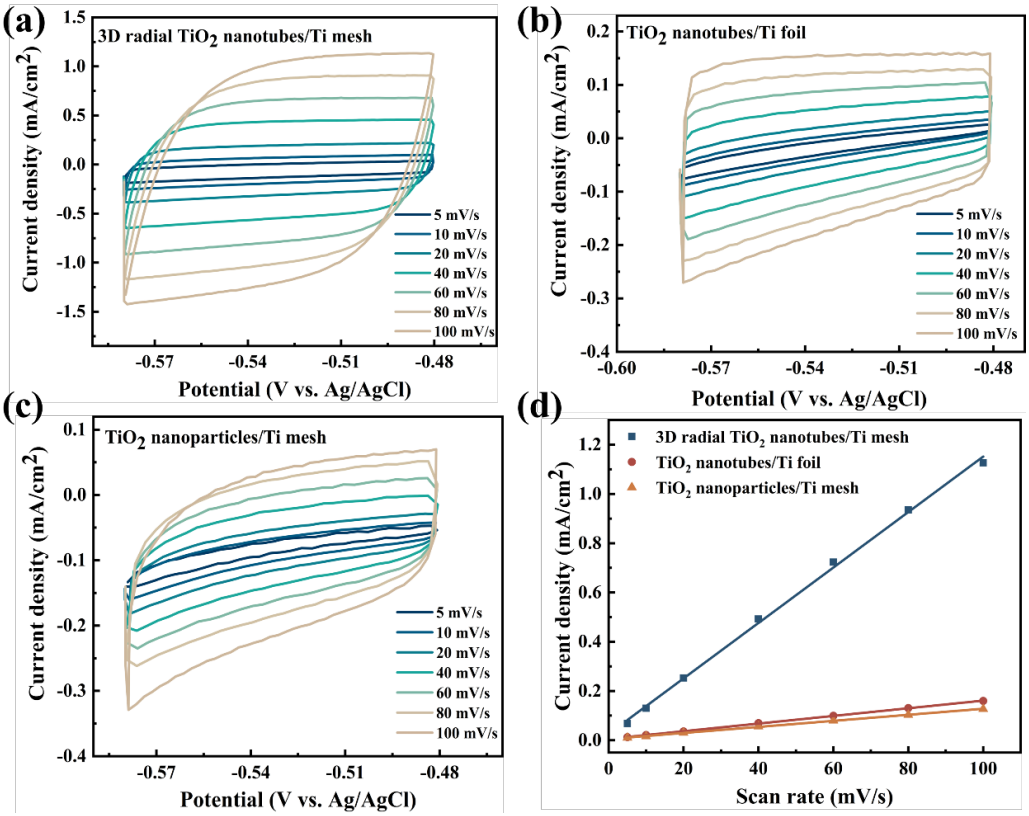

158

159 **Fig. S7** CV curves (vs. Ag/AgCl) for (a) 3D radially-grown TiO_2 nanotubes/Ti mesh
160 photoanode, (b) TiO_2 nanotubes/Ti foil photoanode, (c) TiO_2 nanoparticles/Ti mesh
161 photoanode under various scan rates; (d) Electrochemical surface areas of various
162 photoanodes.

163

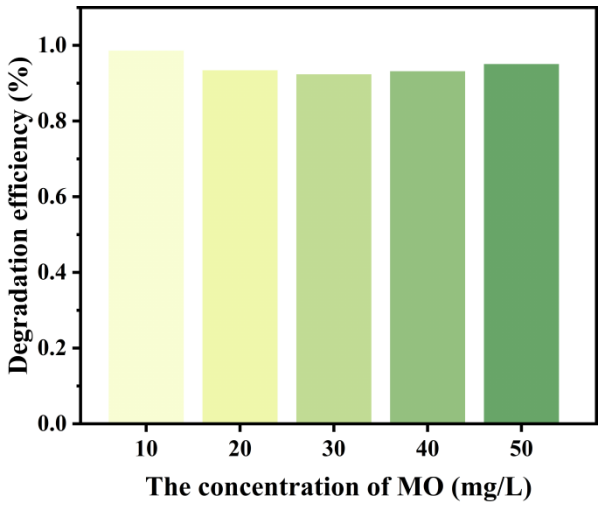

164

165 **Fig. S8** Degradation efficiency of MO by PFC with three-layered TiO_2 nanotubes/Ti
166 mesh photoanode under different initial concentrations.